DE GRUYTER Energy Harvesting and Systems 2016; 3(2): 161–171

B. Geppert* and A. Feldhoff

An Approach to a Flexible Thermoelectric Generator Fabricated using Bulk Materials

DOI 10.1515/ehs-2015-0015

Abstract: A prototype flexible thermoelectric generator fabricated with bulk materials is presented. Mineral-fiber band and copper tape are used as flexible substrate and electric connectors, respectively, to coil up the constructed thermoelectric device under investigation. The applied active thermoelectric materials are $Ca_3Co_4O_9$ ceramic and Cu-Ni alloy for hole and electron conduction, respectively. Thermal parallel and electric series connections of the mentioned materials were realized in the prototype flexible thermoelectric generator. The device delivered an open-circuit voltage of 16.52 mV and a short-circuit current of 19.40 μA with a temperature difference of $\Delta T_{TEG} = 31$ K for the hot side temperature of 420 K. The device exhibits an approximately 3 cm long stripe that include four basic units (n-p pair and electric connector).

Introduction

Studies on thermoelectric systems focus on thermoelectrically active materials and on entire thermoelectric devices that consist of different materials. Hence, thermoelectric investigations are highly interdisciplinary and involve fields ranging from solid state chemistry, for the development of new materials, to fabrication engineering, including geometric and electronic research. The crucial quantities in determining the thermoelectric properties of a material are the isothermal ($\vec{\nabla} T = 0$) specific electric resistivity ρ, the Seebeck coefficient α (from thermovoltage) and the specific entropy conductivity Λ at electric open-circuit conditions ($\vec{j}_q = 0$); see Fuchs (2010, 2014), Feldhoff (2015). The coupled potential gradients for entropy $\vec{\nabla} T$ and charge $\vec{\nabla} \varphi$ and the related generated entropy flux density $\vec{j}_S$ and charge flux density $\vec{j}_q$ can be quantitativily described in terms of thermoelectric quantities, considering a thermoelectric material tensor that includes all of the measurable thermoelectric properties that determine the thermoelectric performance of a particular material. The array presentation for the thermoelectric description is shown in eq. [1]; see Feldhoff (2015), Geppert et al. (2015):

$$\begin{pmatrix} \vec{j}_S \\ \vec{j}_q \end{pmatrix} = - \begin{pmatrix} \frac{\alpha^2}{\rho} + \Lambda & \frac{\alpha}{\rho} \\ \frac{\alpha}{\rho} & \frac{1}{\rho} \end{pmatrix} \cdot \begin{pmatrix} \vec{\nabla} T \\ \vec{\nabla} \varphi \end{pmatrix} \qquad [1]$$

The leg-area related flux densities for the entropy $\vec{j}_S$ and charge $\vec{j}_q$ with the cross-sectional area $\vec{A}_{leg}$ of the regarded legs give the absolute fluxes J_S and J_q according to:

$$J_S = \vec{j}_S \cdot \vec{A}_{leg} \qquad [2]$$

$$J_q = \vec{j}_q \cdot \vec{A}_{leg} \qquad [3]$$

In addition to trying to apply certain materials to certain temperature conditions, the geometric properties of a complete thermoelectric generator (TEG) must be considered. Many studies have considered $Bi_{2-x}Sb_xTe_3$-based materials or metals such as Ni and Cu; see Kuznetsov et al. (2002), Poudel et al. (2008). The construction of a TEG requires an electrical series-connection of a hole conductor ($\alpha > 0$), where the motions of thermal and electric fluxes are directed in the same direction and an electron conductor ($\alpha < 0$), where the thermal and electric fluxes are directed in the opposite directions; see Feldhoff and Geppert (2014). The materials connected in electronic series are called legs and are commonly connected using metallic (e.g., copper) connectors. If the device is placed in a gradient of thermal potential $\vec{\nabla} T$, an electric potential $\vec{\nabla} \varphi$ builds up, and, according to eq. [1], coupled fluxes are generated for the entropy current density $\vec{j}_S$ and electric current density $\vec{j}_q$. In the case of high charge carrier densities (compared with isolating materials), the potential gradients $\vec{\nabla}$ along the length L_{leg} of the applied legs can be expressed as drops (differences) Δ in terms of the considered potentials for entropy and charge.

$$\frac{\vec{\nabla} T}{L_{leg}} = \Delta T \qquad [4]$$

$$\frac{\vec{\nabla} \varphi}{L_{leg}} = \Delta \varphi \qquad [5]$$

Hence, a TEG is a device that transfers energy from an entropy current to an electric current; see Fuchs (2010, 2014), Feldhoff (2015).These properties make a

---

***Corresponding author: B. Geppert,** Institute of Physical Chemistry and Electrochemistry, Leibniz Universität Hannover, Germany,
E-mail: benjamin.geppert@pci.uni-hannover.de
A. Feldhoff, Institute of Physical Chemistry and Electrochemistry, Leibniz Universität Hannover, Germany

thermoelectric generator that is useful for recovering waste heat in different processes.

Most of the current studies on flexible or even coilable thermoelectric systems are based on thin-film or at least thick-film technology. Thin-film fabrication often uses $Bi_{2-x}Sb_xTe_3$, which is the most efficient and prominent system for application in the 300–473 K range; see Cao et al. (2014) and Francioso et al. (2011). Flexible harvesters were also fabricated using metals such as Cu andNi, see Glatz, Munwyler, and Hierold (2006). Studies have also been performedon flexible TEGs using polymer-based composites; see Suemori, Hoshino, and Ka-mata (2013), Stepien et al. (2015).Using bulk materials (pressed and sintered) the physical properties as electric resistivity, thermovoltage and mechanical stability are superior compared to those of deposited versions of the same material. Due to the techniques of thin- or thick-film production, the grains of the materials are not necessarily contacted in either sintered ceramics or metals. Compared to bulk Bi-Te, electrochemically deposited Bi-Te films exhibit higher specific electric resistance values and smaller Seebeck coefficient values; see Yoo et al. (2005). Applying bulk fabrication avoids the requirement for elaborate equipment that is typically required for thin-film fabrication of the thermoelectric materials using techniques such as sputtering, printing or growing (e.g., electrochemical deposition). The contact of grains inside the film can also be a problem for printing. (Bi, Sb)-Te films obtained by screen-printing technologies can exhibit a higher electric resistance compared with that of the bulk material. The films must be densified by cold-pressing to decrease the specific electric resistance and increase the Seebeck coefficient; see Cao et al. (2014).

The present approach allows the inclusion of different material classes, as oxides and metals, without considering the contact of the grains forming the entire bulk phase. Furthermore, the costs of the $Bi_{2-x}Sb_xTe_3$ compounds are higher than those of the materials that we intend to use in our device. A summary of material costs for thermoelectrics is presented by LeBlanc et al. (2014). Conventional systems often include ceramic bottom- and top-plates with the series connection of thermoelectric legs in between. After connecting the legs electrically, the system is closed and can only be opened by disconnecting the assembled materials. Therefore, a coilable TEG exhibits advantagous fabrication. Because the TEG stripe is prepared as a geometrically open system, it is easier to connect the thermoelectric legs to the metallic connector without producing any electric short-circuits that must be avoided. In conventional rigid devices, the prepared electric connectors have to be added very precisely to maximize the leg density. We built devices using both the rigid approach and the flexible approach. In our opinion, upscaling is easier using the approach of first fabricating an open stripe TEG, and then packing it into a dense system (e.g., via coiling up the stripe). Therefore, a stripe TEG is easier to assemble than is a conventional "chess-pattern" geometry. A flexible prototype thermoelectric generator was fabricated using bulk materials. Mineral-fiber band as flexible substrate enables the coiling of the constructed thermoelectric system under investigation. For n-type legs, Cu-Ni alloy was applied, whereas the p-type leg was realized using $Ca_3Co_4O_9$. Cu-tape was used to connect the thermoelectric materials. The increased leg density obtained without risking electric short-circuit conditions (the applied substrate, in this case mineral-fiber band, is the electric isolating layer) is the advantage of coiled TEGs compared with conventional rigid TEGs that have a "chess pattern" geometry. Indeed, flexible TEG constructed with thin-film deposited materials can be compacted to a very high degree. The presented prototype is a macroscopic system that can also be developed at smaller scales.

Experimental

Material Synthesies and Preparation

The p-type thermoelectric oxide $Ca_3Co_4O_9$ was synthesized using the sol-gel method, as described by Feldhoff et al. (2008).Nitrates of calcium and cobalt cations were stoichiometrically added to an aqueous ammonia solution of pH = 9 containing citric acid and EDTA for complexing the solvated metal ions. The obtained precipitate was calcined at 1,073 K for 10 h with a heating and cooling rates of $3K \cdot min^{-1}$. The calcined powder product was cold-pressed and sintered at 1,173 K for 10 h at heating and cooling rates of $2\,K\,min^{-1}$. Bars (legs) with length, width and thickness of 6 mm, 1.5 mm and 1 mm, respectively, were cut from the obtained $Ca_3Co_4O_9$ ceramic-disc.

The Cu-Ni alloy was in the form of a commercially available wire with a diameter of 1 mm. To connect the thermoelectric materials, adhesive Cu-tape was attached on a mineral-fiber band (HORST GmbH; order-nr.: 10 03 02). The thermoelectric materials were mounted to the Cu connectors and attached by a commonly used solder, to obtain the electric series connection, that is essential for the device. Silver paste was used to connect the thermoelectric materials with the Cu connectors through the solder. Silver paste is used to avoid other preparation technologies such as physical vapor deposition (PVD) when coating the ceramic surface with a metallic layer. It is not possible to use the silver paste without soldering, because this leads to the delamination of the silver layer from the Cu surface during heating due to the thermomechanical stresses inside the assembled layer structure. The manufacturer's physical data for applied commercial materials are listed in Table 1. The parameters for the Cu tape were taken from the data sheet prepared by Deutsches Kupfer-Institut e.V. (DKI), see Franke and Juhl (2000). The entropy conductivity at open-circuit conditions Λ is related to the heat conductivity λ via the absolute working temperature T, shown in eq. [6], see Feldhoff (2015).

$$\lambda = T \cdot \Lambda \tag{6}$$

Thermoelectric Measurements of Single Materials

To characterize the thermoelectric properties of the materials, the temperature-dependent isothermal specific electric resistivity and the Seebeck coefficient, as estimated from the thermovoltage, were measured. Using these data the power factor $\frac{\alpha^2}{\rho}$, which is a part of the tensor element, describing the entropy conductivity coupled to the electric phenomenon, in eq. [1], was estimated for each compound. A precision vertical diamond wire-saw model 3242 from O'WELL was used for sample preparation. Thermoelectric properties were measured using a measurement cell constructed in-house that is a modified version of the arrangement described by Indris (2001). The sample is clamped between two platinum electrodes to close the electric circuit in a pseudo-four-point measurement. The applied furnace is an ELITHE thermal system. The electronic parameters were measured with KEITHLEY 2100 $6\frac{1}{2}$ Digit Multimeters. The measured data were converted using the LAB VIEW software. An illustration of the measurement setup for determining the parameters of single materials is presented in Figure 1.

Thermoelectric Measurements of Prototype TEG

The fabricated prototype was placed on a heater to estimate its thermoelectric characteristics. The heat sink was

Table 1: Physical manufacturer's data of applied commercial materials with thermoelectric parameters for 293 K.

material	ρ/mΩcm	λ/W(mK)$^{-1}$	Λ/Wm^{-1}K^{-2}	α/µVK^{-1}	$T_{degradation}$/K
mineral fiber	$10^{17}...10^{18}$	1.0	$3.4 \cdot 10^{-2}$	n.a.	890 (T_{strain})
Cu tape	$1.7 \cdot 10^{-3}$	394	1.3	n.a.	1,356 (T_{melt})
Cu-Ni alloy	$4.9 \cdot 10^{-2}$	23	$7.8 \cdot 10^{-2}$	−40	1,553 (T_{melt})
Sn-Pb solder	$1.4 \cdot 10^{-2}$	50	$1.7 \cdot 10^{-1}$	n.a.	456 (T_{melt})

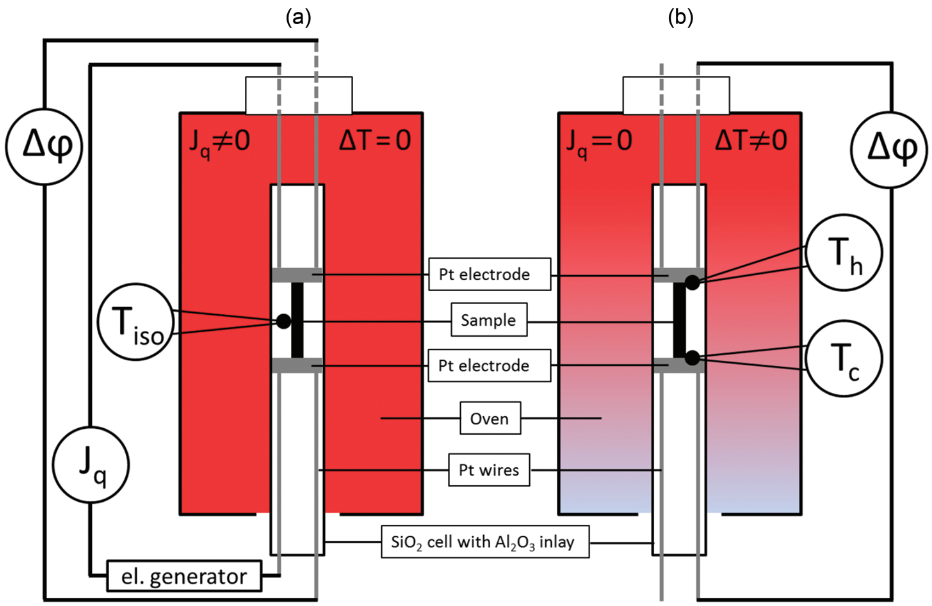

Figure 1: Schematic illustration of the measurement setup for determining the thermoelectric characteristics of single materials.
(a) setup for determining the specific isothermal electric resistance,
(b) setup for determining the Seebeck coefficient.

established naturally, using the temperature drop, that was generated by radiation losses without any additional setup for passive or active cooling. Hence, the temperature of the cold junction of the device increased with the increasing temperature of the hot side (heater side). The used heat-source was a STUART CB160 hot-plate. The prototype TEG was placed on the heater in a bent form as shown in Figure 3(c). A schematic illustration of the measurement setup is shown in Figure 2. The temperature was measured using thermocouples. The thermovoltage $U = \Delta\varphi$ (see eq. [5]) and the electric current $I = J_q$ (see eq. [3]) were measured for different external load R_{load}-values.

Microstructure Analysis

The materials were analyzed using field-emission scanning electron microscopy (FE-SEM) using a JEOL JSM-6700F, equipped with an Oxford Instruments INCA 300 energy-dispersive X-ray spectrometer (EDXS) for elemental analysis. The phase composition of $Ca_3Co_4O_9$ calcined powder product and sintered ceramic were analyzed by X-ray diffraction (XRD) using a Bruker D8 Advance with Cu-K_α radiation. The reference data for the crystal structure analysis were taken from the Powder Diffraction File (PDF2) database.

Fabrication of the Flexible Thermoelectric Generator

Figure 3 shows the fabricated device as a flat stripe and in perspective view to show the provided flexibility. The basic material of the developed generator is a mineral-fiber band that provides a flexible substrate for the TEG stripe. The band is 14.5 mm wide and 150 μm thick and can be heated to 890 K in continuous working conditions.

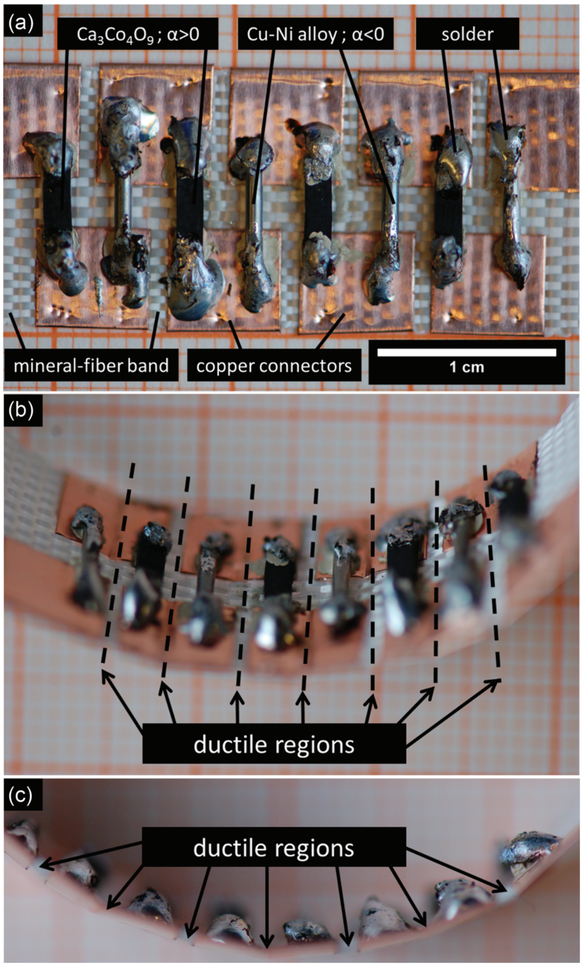

Figure 3: Microphotography of the prototype flexible TEG; (a) side view on plan side, (b) perspective view on bend device, (c) top view on bend device.

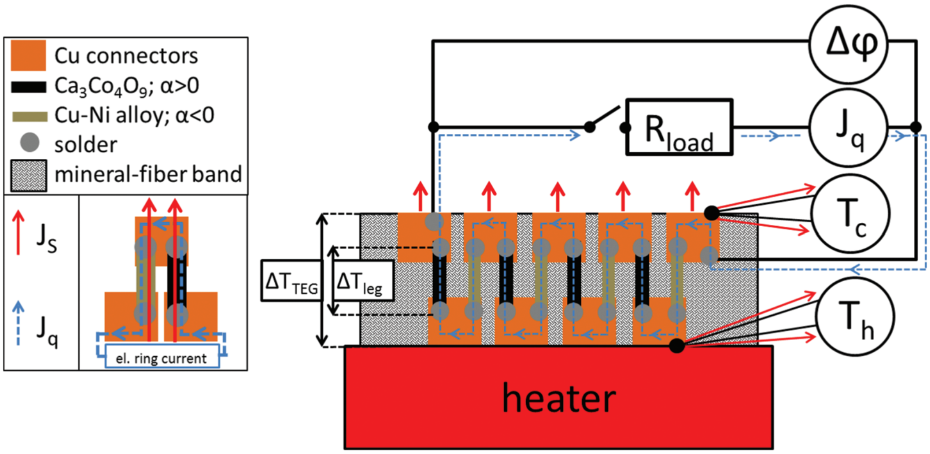

Figure 2: Schematic side-view illustration of the measurement setup for determining the thermoelectric characteristics of the flexible TEG. Schematics for a device with parallel entropy current J_S (see eq. [2]) and electric ring current J_q (see eq. [3]) are displayed.

The copper tape, used to realize the electric series connection, has a width of 6.3 mm and a thickness of 50 μm. It was attached with its adhesive side to the mineral-fiber band substrate by clamping it around the edge of the band such that there was approximately 1 mm of free space between each pair of Cu stripes. The gap between the connectors of the two sides (hot and cold sides in working conditions) is approximately 2.5 mm. The $Ca_3Co_4O_9$ ceramic legs were cut from a sintered disc of the $Ca_3Co_4O_9$ material. Each p-type leg exhibits a length of 6 mm, a width of 1.5 mm and a thickness of 1 mm. The metallic Cu-Ni alloy was used in the form of a wire with a diameter of 1 mm. The wire was also cut into pieces with a length of 6 mm. To fix the thermoelectric legs to the copper connectors, the materials were initially coated with silver paste that had been cured at room temperature. The legs were then soldered to obtain a mechanically stable connection.

To examine the inside of the fabricated device, a basic unit was cut out and embedded in epoxy resin to fix the thin and flexible part of the device. A cross-section was then obtained by cutting and polishing the assembled materials. A photograph of the cross-section of the prepared basic unit is shown in Figure 4. With the exception the silver paste all components of the prepared basic unit of the prototype flexible TEG can be seen. Related to the prepared cut, the Cu-Ni alloy wire is completely surrounded by the used solder (right side of the basic unit). The ceramic $Ca_3Co_4O_9$ material is not completely surrounded by the solder (left side of the basic unit). Due to the location of the prepared cut for the cross-section, only one piece of the solder remains, that is positioned on the upper left edge of the $Ca_3Co_4O_9$ sample bar. Despite of the impression conveyed by the arrangement shown in Figure 4, all connecting regions of thermoelectric materials and the Cu connectors were coated completely with solder and provided a mechanically stable fixation, see Figure 3. Figure 4(b), 4(c) show pseudocolor micrographs with the displayed colors related to the energy-ranges are displayed to identify the materials used in the basic unit arrangement. The epoxy resin, surrounding the basic unit, is displayed in orange-red as caused by the X-ray emission of the carbon (C: K-emission) with an emission energy in the 0–0.5 keV range. The electric connectors (Cu: L-emission) and the Cu-Ni alloy (Cu, Ni: L-emission) are shown in yellow with an X-ray energy range of 0.5–1.0 keV. The mineral-fiber band (Si, Al: K-emission) is colored green and is related to an energy range of 1.0–2.0 keV. The solder (Sn, Pb: L, M-emission) and the silver paste (Ag: L-emission) are displayed in light blue with related X-ray emissions covering the 1.5–5 keV energy range.

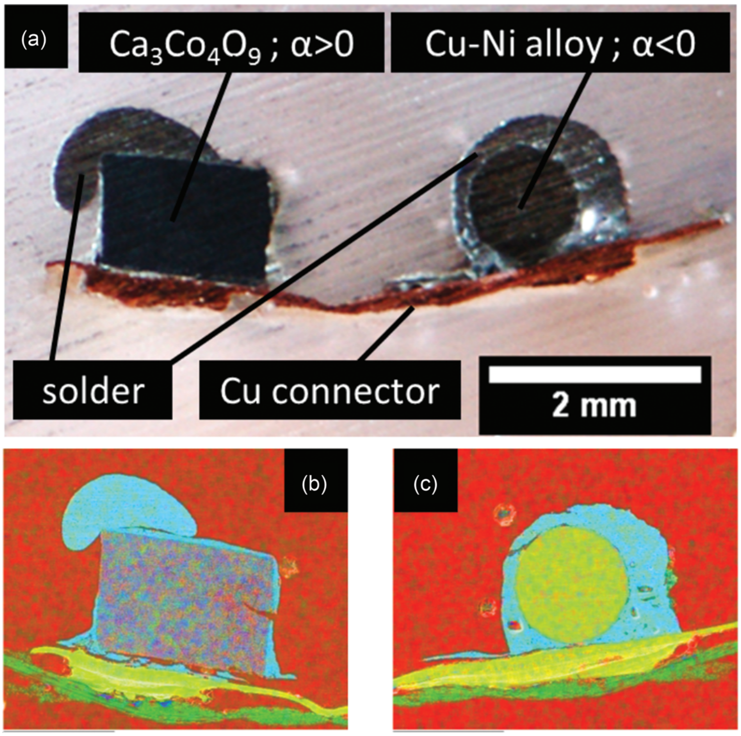

Figure 4: (a) Microphotograph of cut and polished cross-section of the prepared basic unit surrounded by epoxy resin (mineral-fiber band is not visible); (b) pseudocolor micrograph of $Ca_3Co_4O_9$ side; (c) pseudocolor micrograph of Cu-Ni alloy side. Light blue: Sn, Pb, Ca and Ag (solder and Ag-paste); green: Si, Ca and Al (mineral-fiber band); yellow: Cu and Ni (electric connector and Cu-Ni alloy); purple: Co and Ca (p-type semiconductor); orange-red: C (epoxy resin).

For the ceramic material $Ca_3Co_4O_9$ the mixture of pseudocolors results in purple color (Ca, Co: L, K-emission). The additional energy ranges are for Ca (orange-red) with an energy range of 0–0.5 keV and for Co (blue) with an energy range of 6.0–9.0 keV.

Figure 5 shows the area-related elemental distributions of the cut and polished cross-section of the prepared basic unic. The detailed results for elemental distribution of each element are presented.

The interface of the ceramic $Ca_3Co_4O_9$ and the metallic solder, interconnected with the silver paste, is the most fragile part of the device. Although the connection of the Cu-Ni alloy and the copper connector, realized by silver paste and solder, is still intact after the preparation, the ceramic $Ca_3Co_4O_9$ is delaminated from the copper tape. The difference in physical surface properties of ceramic material and metallic components leads to the poor mechanical stability of the hetero-material boundary region. The disconnection can

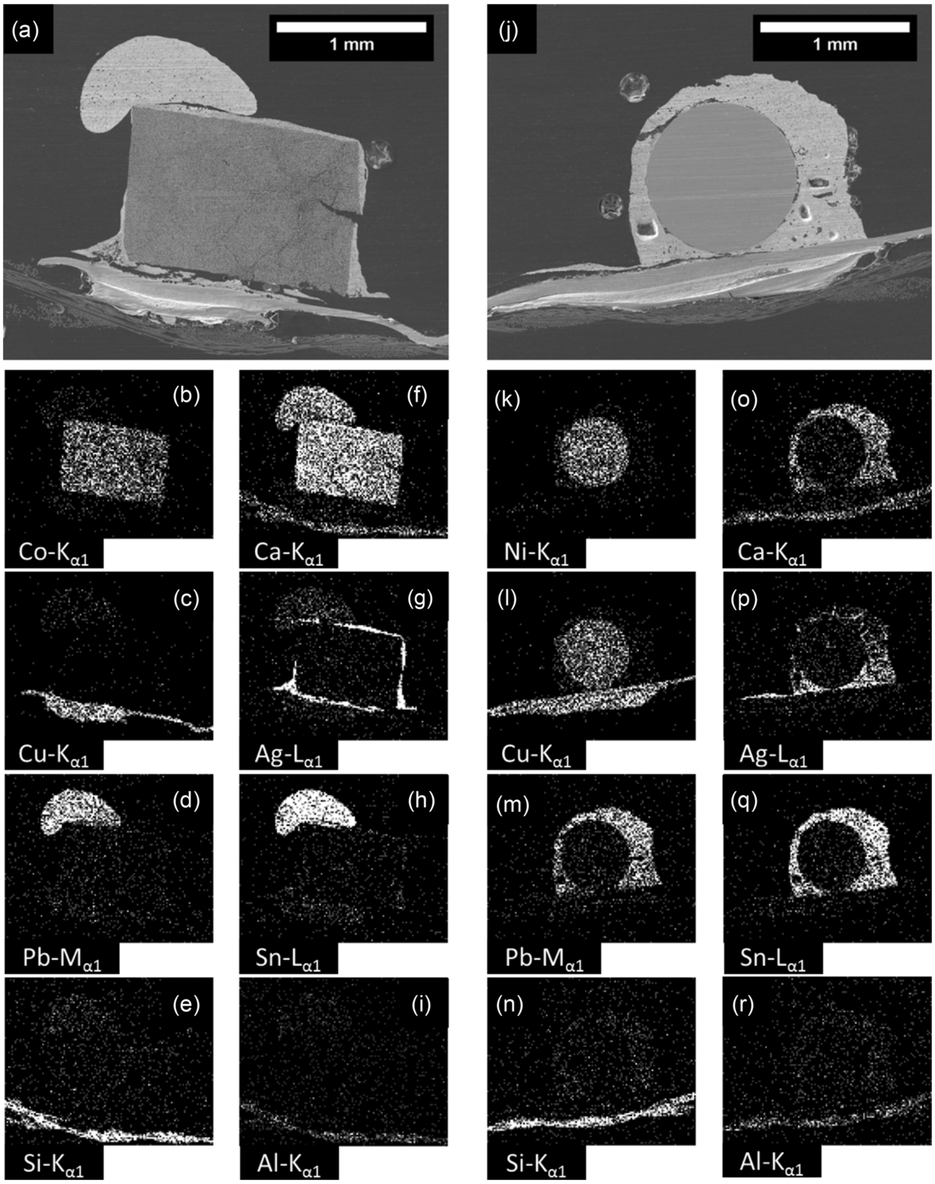

Figure 5: EDXS elemental maps of cut and polished cross-section of the prepared basic unit: (a) Secondary electron micrograph of the $Ca_3Co_4O_9$ side, (b)–(i) elemental distribution at the $Ca_3Co_4O_9$ side; (j) Secondary electron micrograph of the Cu-Ni alloy side; (k)–(r) elemental distribution at the Cu-Ni alloy side.

be caused by the mechanical preparation and heating of the device until the melting point of the solder.

Results and Discussion

Microstructure of Materials and Compositions

The crystal structures of the calcined powder product and the sintered p-type $Ca_3Co_4O_9$ ceramic were analyzed by X-ray diffraction. The diffractograms are shown in Figure 6. Neiter $Ca_3Co_4O_9$ calcined powder nor the sintered ceramic show any phases other $Ca_3Co_4O_9$. The relative intensities of the detected reflections change from calcined powder to sintered oxide ceramic such that only 00*l* and 20*l* reflections remain. This indicates a texture where plate-like grains are lying preferentially with their crystallographic c-axis normal to the surface of the sintered ceramic, as shown in Figure 8. Such a textured surface structure is caused by the cold pressing during the preparation for the sintering process. The Bragg positions in Figure 6 were taken from the Powder Diffraction Files (PDF2) database.

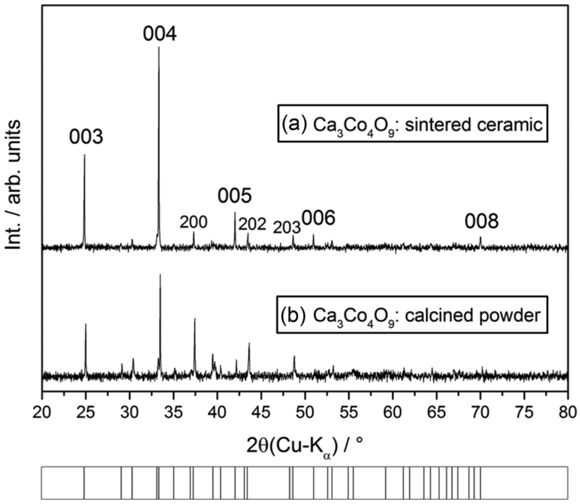

Figure 6: XRD analysis of semi-conducting $Ca_3Co_4O_9$ with displayed Bragg positions underneath (PDF number: 00-058-0661); (a) powder product calcined at 1,073 K for 10 h; (b) textured surface of the ceramic sintered at 1,173 K for 10 h.

Figure 7 shows the elemental compositions of the thermoelectric $Ca_3Co_4O_9$ ceramic and Cu-Ni alloy materials by EDXS method in the FE-SEM. The quantitative analysis of the metals inside the Cu-Ni alloy, Figure 7(b), reveals Cu, Ni and Mn fractions of 57.89 wt.%, 41.11 wt.% and 1.00 wt.%, respectively. Cu-Ni alloys of this elemental composition typically exhibits an almost constant electric resistivity over a wide temperature range (Constantan, Isotan); this is confirmed by an inspection of Figure 10; see Lide (2008). Figure 8 shows a secondary electron micrograph of the surface microstructure for the semiconducting p-type $Ca_3Co_4O_9$. Due to the oriented crystal growth during the sintering process, the grains at the outermost surface of the sintered ceramic show a plate-like morphology. The surface structure exhibits a median grain width of 2.5 μm and a median thickness of the crystal plates of 1.3 μm. The ceramic is not sintered to a dense body. The porous arrangement inside the ceramic can be expected to provide a low thermal conductivity; see Rhee (1975).

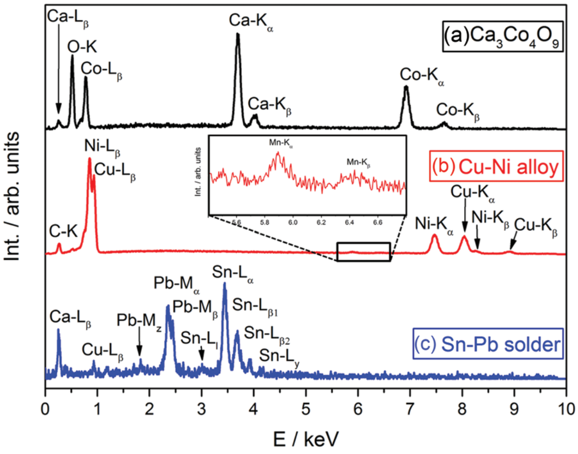

Figure 7: EDX spectra of synthesized and prepared materials. (a) sintered $Ca_3Co_4O_9$ ceramic, (b) Cu-Ni alloy with magnifed view of Mn-$K_{\alpha,\beta}$ signals, (c) applied Sn-Pb based solder.

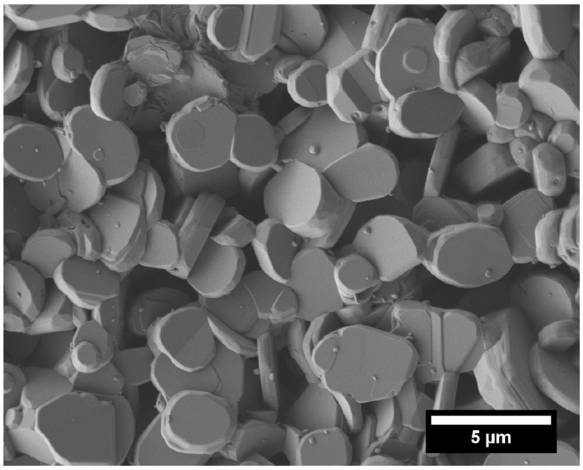

Figure 8: Secondary electron micrograph of the textured $Ca_3Co_4O_9$ surface (see Figure 6 for XRD analysis) after sintering at 1,173 K for 10 h. Note the different magnification compared with Figure 5.

Thermoelectric Investigations

The experimental errors for measurements of the Seebeck coefficients and for the isothermal specific electric resistivities were estimated by considering the errors for sample's geometry measurements, fluctuations of electrical quantities and fluctuations in the temperature profile for the measurement of each material. Based on these considerations, we developed a reliability range for each measurement. Figure 9 shows the obtained Seebeck coefficients of the $Ca_3Co_4O_9$ ceramic and the Cu-Ni alloy.

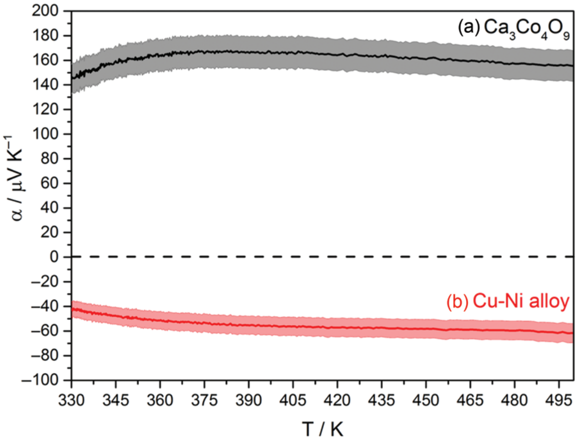

Figure 9: Measured Seebeck coefficients of applied thermoelectric materials as a function of temperature with estimated error ranges. (a) $Ca_3Co_4O_9$ ceramic; (b) Cu-Ni alloy.

The Seebeck coefficients of analyzed materials depend only weakly on temperature. The absolute value of the semiconducting oxide Seebeck coefficient is nearly three times higher than that of the used metallic thermoelectric material. The Seebeck coefficients decreased sharply at approximately room temperature (300 K) due to the vanishing temperature difference along the samples that (not shown). We therefor decided to display the values starting at 330 K and to show the values in the range for with we have reliable measurement data. The Seebeck coefficient of the ceramic material is almost three times higher than the value for the Cu-Ni alloy. The Seebeck coefficient of the Cu-Ni alloy reaches values in the range between –40 and –60 μVK^{-1} at roomtemperature (300 K). This result is in good agreement with the values obtained in round-robin measurements reported by Lu et al. (2009) Lu, Lowhorn, Wong-Ng, Zhang, Lu, Otani, Thomas, Tran, Dilly, Ghamaty, Elsner, Hogan, Downey, Jie, Li, Obara, Sharp, Caylor, Venkatasubramanian, Willigan, Yang, Martin, Nolas, Edwards, and Tritt and Lowhorn et al. (2009) Lowhorn, Wong-Ng, Zhang, Lu, Otani, Thomas, Tran, Dilly, Ghamaty, Elsner, Hogan, Downey, Jie, Li, Obara, Sharp, Caylor, Venkatasubramanian, Willigan, Yang, Martin, Nolas, Edwards, and Tritt. For the Seebeck measurements of the $Ca_3Co_4O_9$, the values are 10–20 μVK^{-1} higher than those obtained at 300 K by Miyzaki (2004).

Figure 10 shows the results for isothermal specific electric resistivity ρ measurements of applied thermoelectric materials as a function of temperature. The isothermal specific resistivities of ceramic $Ca_3Co_4O_9$ are in the expected range for this semiconducting oxides. The measurement results are on the same order of magnitude as those presented in Miyzaki (2004). The absolute values are 3 to 4 times higher. For the Cu-Ni alloy, the isothermal specific resistivity is almost independent of the temperature in the considered temperature range. This was already expected from elemental analyses (see discussion of Figure 7(b)). The isothermal specific resistivitiy values of the Cu-Ni alloy match those reported in the manufacturer's datasheet.

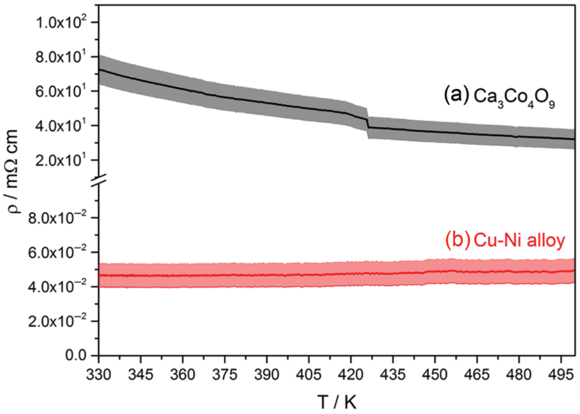

Figure 10: Measured isothermal specific electric resistivities of applied thermoelectric materials as function of temperature with estimated error ranges. (a) $Ca_3Co_4O_9$ ceramic; (b) Cu-Ni alloy.

The power factors $\frac{\alpha^2}{\rho}$ for both materials were calculated from the median values of measured electric resistances and Seebeck coefficient data and are displayed in Figure 11. The error range was received by error propagation from determined errors for the single parameters of the Seebeck coefficients α (see Figure 9) and the specific resistivities (see Figure 10).

To determine the thermoelectric parameters of the flexible prototype TEG, four temperature differences ΔT were established, as indicated in Table 2 and Figure 12. Figure 12(a) shows voltage-current (U-I) characteristics with a good agreement between the measured data (data points) and the linear fit (solid lines). Note, that the slopes of the lines correspond to the internal resistance R_{TEG}, as indicated in

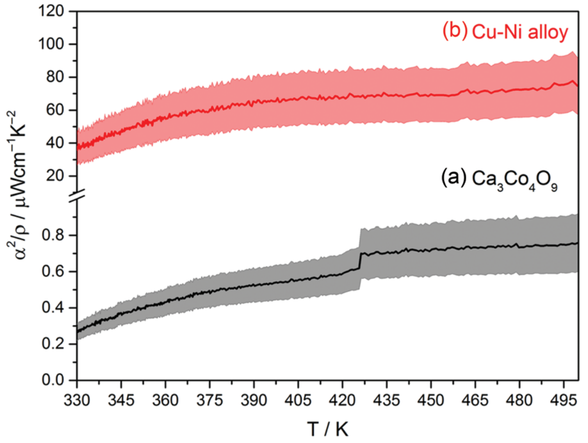

Figure 11: Power factors estimated from measured isothermal specific electric resistivities and Seebeck coefficients as function of temperature with estimated error ranges obtained from error propagation related to errors shown in Figures 9 and 10. (a) $Ca_3Co_4O_9$ ceramic; (b) Cu-Ni alloy.

Table 2: Determined thermoelectric parameters of the prototype flexible TEG for different temperature conditions.

T_h/K	ΔT_{TEG}/K	T_{median}/K	R_{TEG}/Ω	$P_{el,\,max}$/nW	U_{oc}/mV	I_{sc}/μA
420	31	404	851.61	82.00	16.52	19.40
361	22	350	909.91	14.56	7.29	8.01
336	16	328	885.94	4.65	4.06	4.58
307	7	304	715.90	0.24	0.88	1.23

Table 2. The electric output power P_{el} was estimated in terms of different load resistivities R_{load}. Figure 12(b) also shows the electric output power-electric current (P_{el}-I) characteristics, with good agreement observed between the measured data (data points) and the parabolic fit (solid lines).

The values of the open circuit voltage U_{OC} calculated from the measured Seebeck coefficients α (see Figure 9) of single materials, are considerably larger. This is likely due to large differences between the temperature drop of the entire device from the heat source to heat sink ΔT_{TEG} and the established temperature difference along the legs of a basic unit $\Delta T_{basicunit} = \Delta T_{leg}$ (see Figure 2). Table 3 presents the calculated temperature differences along the legs of a basic unit $\Delta T_{basicunit}$ related to the measured Seebeck coefficients (see Figure 9) and open circuit voltages for the basic unit $U_{OC,\,basicunit}$. The data collected for the hot side temperature of $T_h = 336$K and the temperature difference along the entire TEG, $\Delta T_{TEG} = 7$K, were not considered, because the measured values for the Seebeck coefficients for the single materials in this temperature range are not reliable (see Figure 9 and related discussion).

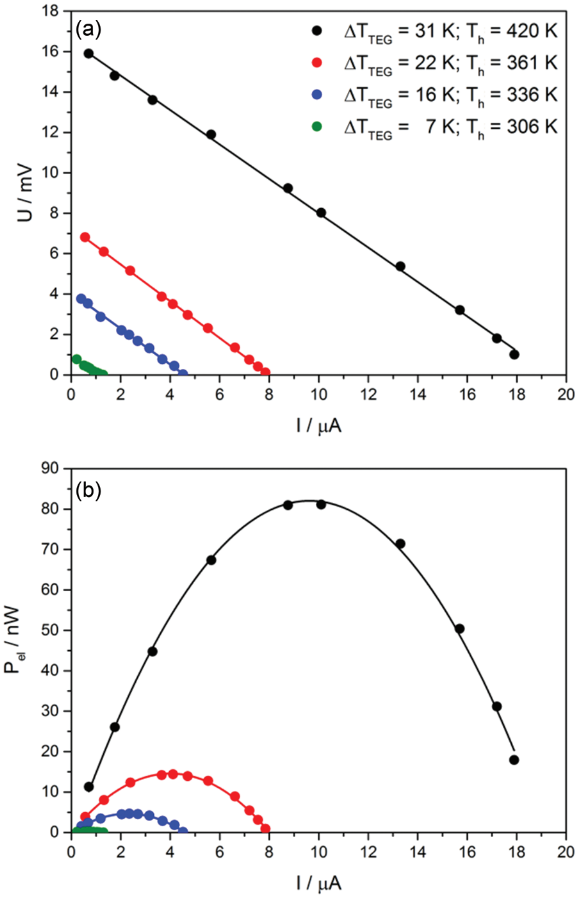

Figure 12: Thermoelectric properties of the prototype flexible TEG (four basic units, see Figure 3 for length of the device). (a) Voltage over electric current for four different temperature conditions. (b) Power-current characteristics for four different temperature conditions.

Table 3: Calculated and measured temperature distributions inside the device.

T_h/K	ΔT_{TEG}/K	$\Delta T_{basicunit}$/K	$\alpha_{basicunit}$/μVK^{-1}	$U_{OC,\,basicunit}$/mV	$\frac{\Delta T_{basicunit}}{\Delta T_{TEG}}$/%
420	31	19	222.25	4.13	61.29
361	22	9	211.06	1.82	40.91
336	16	6	182.13	1.02	37.50

Large parasitic heat losses are present along the device's hot and cold sides and are likely caused by the mineral-fiber substrate. The contact area between the copper-tape and the mineral-fiber band appears to be too large. The mineral-fiber band has to be more slim such that the amount of integrated copper can be reduced to minimize this contact areas. The thermal short-circuited situation can also be caused by the Cu-Ni alloy, which exhibits a larger thermal conductivity compared with the fiber

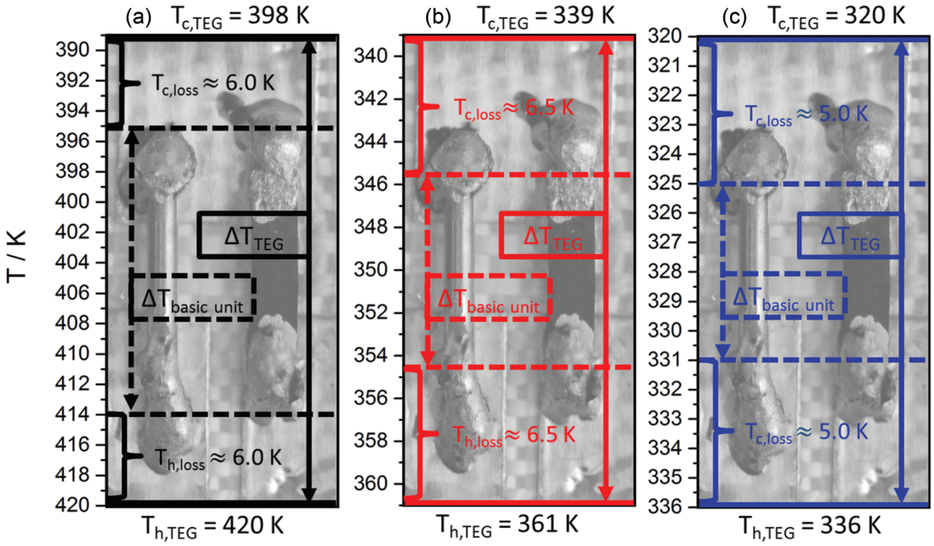

Figure 13: Temperature distributions inside the TEG with displayed thermal losses for hot side $T_{h,loss}$ and cold side $T_{c,loss}$ of the entire TEG.

substrate (see Table 1). The alloy must be the main origin of the parasitic heat losses via thermal short circuiting. Figure 13 illustrates the temperature distributions across the hot and cold sides of the device relative to the hot side temperature.

Conclusions

The prototype TEG displays flexibility that is only limited by the applied pieces of ductile copper-tape as electric connectors. The limiting factor for the heating of the device is the solder, which melts between 423 and 473 K. Because of the less heat proofed Sn-Pb solder the prototype can not be applied to temperatures above the decomposition temperature of BiTe. Related to the other materials in the device a reasonable temperature range for application should be up to 890 K (degeneration temperature of the mineral-fiber band). The solder also limits the current because of a very high boundary resistivity at the connecting regions of metallic solder and semiconducting p-type oxide. The geometrical arrangement of the applied materials provides variation of thermoelectric materials while maintaining the mechanical flexibility of the TEG. Metals and alloys as well as ceramics can be integrated in the fabrication process. The joining of dissimilar materials is the major concern. It is therefore important to investigate alternatives to soldering for attaching non-metallic materials to metallic connectors. It is also important to investigate the use of a solder with a higher melting point, such as a Sn-Sb solder, to improve the thermal stability of the entire device. To join ceramic materials to metallic connectors, alternative solutions must be applied to avoid preparation techniques such as physical vapor deposition (PVD). Epoxy resin including metal particles for electric conduction should be tested.

The observed parasitic heat losses are likely caused by the large area of the copper-tape that can transport the heat to the mineral-fiber substrate. The substrate material should be thinner in order to decrease the thermal conduction. To decrease the thermal losses, the width of the substrate material must be smaller to minimize the gap between the hot side of the generator and the hot side of the thermoelectric junctions related to the thermoelectric legs.

Here a symmetric approach to fabrication was used. The legs were centered between the hot and the cold sides of the entire device. This architecture leads to disadvantages for temperature distributions during working conditions. Instead, an asymmetric architecture, in which the legs are placed as near as possible to the hot side using a smaller Cu connector while the Cu connector of the cold side should exhibit a larger area to act as passive cooling system. It is expected that constructing the flexible TEG stripe in such an asymmetric fashion would reduce the parasitic heat losses from the heat source to the hot junction of the thermoelectric materials. For the short piece of the presented prototype it is indeed nearly impossible to integrate an effective heat exchanger. For an upscaled and coiled up version of the prototype it is expected, that the mechanical stability suffice to place a cooler onto the device. Another imaginable possiblity to integrate heat exchanger are miniaturized heat-pipes that are clamped to the electric connectors of each basic unit. For application a thermoelectric energy harvesting device a heat exchanger is considered to be essential.

References

Cao, Z., E. Koukharenko, R. Torah, J. Tudor, and S. Beeby. 2014. "Flexible Screen Printed Thick Film Thermoelectric Generator with Reduced Material Resistivity." *PowerMEMS* 557 (012016):1–5. Conference Series.

Feldhoff, A. 2015. "Thermoelectric Material Tensor Derived From the Onsager – De Groot – Callen Model." *Energy Harvesting and Systems* 2 (1):5–13.

Feldhoff, A., M. Arnold, J. Martynczuk, T. Gesing, and H. Wang. 2008. "The Sol-Gel Synthesis of Perovskites by EDTA/Citrite Complexing Method Involves Nanoscale Solid State Reactions." *Solid State Sciences* 10:689–701.

Feldhoff, A., and B. Geppert. 2014. "A High-Temperature Thermoelectric Generator based on Oxides." *Energy Harvesting and Systems* 1 (1–2):69–78.

Francioso, L., C. D. Pascali, I. Farella, C. Martucci, C. Creti, P. Siciliano, and A. Perrone. 2011. "Flexible Thermoelectric Generator for Ambient Assisted Living Wearable Biometric Sensors." *Journal of Power Sources* 196:3239–43.

Franke, H., and K. Juhl. 2000. *Kupfer in Der Elektrotechnik-Kabel Und Leitungen*. Duesseldorf, DE: Breuerdruck. Internet Version 2000.

Fuchs, H. 2010. *The Dynamics of Heat – a Unified Aproach to Thermodynamics and Heat Transfer*, 2nd edn. New York: Springer. Graduate Texts in Physics.

Fuchs, H. 2014. "A Direct Entropic Approach to Uniform and Spatially Continuous Dynamical Models of Thermoelectric Devices." *Energy Harvesting and Systems* 1 (3–4):253–65.

Geppert, B., D. Groeneveld, V. Loboda, A. Korotkov, and A. Feldhoff. 2015. "Finite-Element Simulations of a Thermoelectric Generator and Their Experimental Validation." *Energy Harvesting and Systems* 2 (1):95–104.

Glatz, W., S. Munwyler, and C. Hierold. 2006. "Optimisation and Fabrication of Thick Flexible Polymer Based Micro Thermoelectric Generator." *Sensors and Actuators, A* 132:337–45.

Indris, S. 2001. *Perkolation Von Grenzflächen in Nanokristallinen Keramischen Kompositen – Li-Ionenleitfähigkeit UndLi-NMR-Relaxation*. Göttingen, DE: Cuvillier Verlag. Dissertation.

Kuznetsov, V. L., L. A. Kuznetsova, A. E. Kaliazin, and D. M. Rowe. 2002. "High Performance Functionally Graded and Segmented-based Materials for Thermoelectric Power Generation." *Journal of Materials Science* 37:2893–7.

LeBlanc, S., S. K. Yee, M. L. Scullin, C. Dames, and K. E. Goodson. 2014. "Material and Manufacturing Cost Considerations for Thermoelectrics." *Renewable and Sustainable Energy Reviews* 32:313–27.

Lide, D. 2008. *CRC Handbook of Chemistry and Physics*, 89th edn. Boca Raton, FL: CRC Press. Internet Version 2009.

Lowhorn, N. D., W. Wong-Ng, W. Zhang, Z. Q. Lu, M. Otani, E. Thomas, M. G. T. N. Tran, N. Dilly, S. Ghamaty, N. Elsner, et al. 2009. "Round-Robin Measurements of Two Candidate Materials for a Seebeck Coefficient Standard Reference Material." *Applied Physics A* 94:231–4.

Lu, Z. Q. J., N. D. Lowhorn, W. Wong-Ng, W. Zhang, Z. Q. Lu, M. Otani, E. Thomas, M. G. T. N. Tran, N. Dilly, S. Ghamaty, et al. 2009. "Statistical Analysis of a Round-Robin Measurement Survey of Two Candidate Materials for a Seebeck Coefficient Standard Reference Material." *Journal of Research of the National Institute of Standards and Technology* 114:37–55.

Miyzaki, Y. 2004. "Crystal Structure and Thermoelectric Properties of the Misfit-Layered Cobalt Oxides." *Solid State Ionics* 117:463–7.

Poudel, B., Q. Hao, Y. Ma, Y. Lan, A. Minnich, B. Yu, X. Yan, D. Wang, A. Muto, D. Vashaee, et al. 2008. "High-Thermoelectric Performance of Nanostructured Bismuth Antimony Telluride Bulk Alloys." *Science* 320:634–8.

Rhee, S. 1975. "Porosity-Thermal Conductivity Correlation for Ceramic Materials." *Materials Science and Engineering* 20:89–93.

Stepien, L., A. Roch, S. Schlaier, I. Dani, A. Kiriy, F. Simon, M. v. Lukowicz, and C. Leyens. 2015. "Investigation of the Thermoelectric Power Factor of KOH Treated PEDOT:PSS Dispersions for Printing Applications." *Energy Harvesting and Systems* 2:1–11.

Suemori, K., S. Hoshino, and T. Kamata. 2013. "Flexible and Lightweigt Thermoelectric Generators Composed of Carbon Nanotube-Polystyrene Composites Printed on Film Substrate." *Applied Physics Letter* 103 (153902):1–4.

Yoo, B. Y., C.-K. Huang, J. R. Lim, J. Herman, M. A. Rayn, J.-P. Fleurial, and N. V. Myung. 2005. "Electrochemically Deposited Thermoelectric n-Type Thin Films." *Electrochimica Acta* 50:4371–7.